*Manuscript (including Abstract)
Click here to view linked References

Impedimetric detection of *Pseudomonas aeruginosa* attachment on flexible ITO-coated polyethylene terephthalate substrates

Lakshmi Deepika Bharatula[a,b], Enrico Marsili[b,c,d,*], and James J. Kwan[a,*]

[a]*School of Chemical and Biomedical Engineering, Nanyang Technological University, Singapore, 637459*

[b]*Singapore Centre for Environmental Life Sciences Engineering, Nanyang Technological University, Singapore, 637551*

[c]*Department of Chemical and Materials Engineering, Nazarbayev University, Astana, Kazakhstan, 010000*

[d]*The Environment & Resource Efficiency Cluster (EREC), Nazarbayev University, Astana, Kazakhstan, 010000*

**Corresponding author: Tel: +65 6514 1222;*

E-mail: jameskwan@ntu.edu.sg and *enrico.marsili@nu.edu.kz*

ABSTRACT:

Biofilm monitoring in environmental and biomedical applications remains a challenge. Conventional biochemical methods do not yet provide a quick quantitative measure of attached biomass. Thus, there is a need for rapid *in situ* detection tools for routine biofilm characterization. Electrochemical impedance spectroscopy (EIS) characterizes the electroactivity of bacteria within a biofilm and has been extensively used to monitor strong electroactive biofilms. Yet, studies on weak electricigens such as *Pseudomonas aeruginosa* remain underrepresented. Here, conductive indium tin oxide coated polyethylene terephthalate (ITO:PET) sheets were used as flexible growth substrates instead of more conventional carbonaceous or gold materials. EIS was compared with standard optical methods for the detection of *P. aeruginosa* biofilms formed on ITO:PET under static growth conditions. Relaxation time analysis showed a dominant time constant at approximately 1

second and confirmed the validity of a two time constant equivalent circuit model for the biofilm impedance. The interfacial resistance calculated from the equivalent circuit analysis showed a rapid drop after bacterial attachment whereas capacitance of the biofilm was masked by the capacitance of ITO:PET. The trends for interfacial resistance and capacitance were independent to the geometry of the ITO:PET working electrode. Moreover, most robust behaviour was observed for rectangular electrodes. EIS across a broad range of potentials with and without inhibitors showed a marked difference between the interfacial resistance of viable and energy inhibited biofilms. Moreover, EIS of exopolysaccharide Δpsl mutant showed a substantial drop in current. Overall, our results indicated that EIS enabled the detection of biofilm formation across large surface areas as early as 24 hours for the weak electroactive species *P. aeruginosa* using a flexible polymeric substrate.

Keywords: Biofilm; ITO:PET; Electrochemical impedance spectroscopy; *Pseudomonas aeruginosa*

1. Introduction

Biofilms are aggregates of microorganisms embedded in a self-produced biofilm matrix consisting of polysaccharides, extracellular proteins, and DNA fragments collectively known as extracellular polymeric substances (EPS) [1]. The EPS forms during the transition from free-swimming cells to a microstructured community attached to a surface [2]. Furthermore, biofilms harbour antimicrobial and antibiotic-resistant strains as well as physiologically differentiated cells (e.g., persisters) that often cause hard to treat chronic infections [3]. Considering the challenges associated with biofilms, methods to monitor their growth and development are needed.

Current biofilm monitoring strategies rely on optical techniques such as microscopy, spectrophotometry, flow cytometry, and fluorescence *in situ* hybridization [4–7]. Although these techniques provide information on bacterial concentration, biofilm microstructure, and biofilm microbial ecology, they are time-consuming, expensive, and not suitable for rapid, *in situ* biofilm detection over large surface areas. Recently, electrochemical impedance spectroscopy (EIS) has been used to monitor biofilm development *in situ* [8–11]. The technique has garnered attention due to the low-cost setup and the ability to quickly monitor large surface areas pertinent to industrial and medical applications. Thorough analysis of EIS results recorded at a range of frequencies and potentials provides information on the extracellular electron transfer (EET) between the electrolyte and an electrode in the presence of a biofilm interface. [12,13].

EET is typically measured for highly electroactive microorganisms such as *Geobacter sulfurreducens* and *Shewanella oneidensis*, which give a strong signal through direct electron transfer via transmembrane cytochromes and conductive pili or via secreted redox mediators (e.g., flavins for *S. oneidensis*) [12,14–16]. Whereas, weak electroactive biofilms such as

Pseudomonas aeruginosa undergo EET via redox probe (self-secreted or exogenous)[17]. Furthermore, EET in EIS specifically gives information on the charge/electron transfer, capacitance and diffusion limitations. Charge transfer corresponds to the redox reactions at the electrode-biofilm interface. Biofilm capacitance is primarily associated with the thickness and the surface coverage of the biofilm attached [13,18,19]. Additionally, the electrode properties such as porosity, surface roughness, surface area and atomic-scale heterogeneity affect the capacitance measurement [13,20]. Moreover, mass diffusional characteristics of charges from bulk to electrode specifically diffusion coefficient and diffusion length are determined by diffusion element [21].

Most studies tend to investigate EIS behaviour on ideal, rigid substrates such as carbon, platinum, and gold [19,22,23]. These substrates have large electrical conductivity and smooth surfaces, which allows for better EIS characteristics and, and thus higher sensitivity for biofilm monitoring compared to polymeric substrates. Yet for many applications, biofilms may contaminate polymeric surfaces across large surface areas (> 200 mm^2), which may assume a number of different geometries. Polymeric substrates such as polyethylene terephthalate (PET) are of particular interest due to their use in food packaging, bottling, medical device packaging, and artificial implants [4,24,25]. PET's conductive counterpart, indium tin oxide coated PET (ITO:PET) has also been actively researched for applications in biomedical devices and flexible optoelectronics [26,27]. These polymer films are prone to contamination from biofilm-forming bacteria, which cause biofouling in packaging industries [28] and pose serious risks in biomedical settings [29,30]. Few reports to date have utilised EIS to study the adhesion of bacteria and biofilm formation on ITO-based substrates [31,32]. Additionally, these studies were performed on glass-based substrates and were limited to initial bacterial adhesion.

We extended our investigation in the present study to *P. aeruginosa* biofilm growth and maturation over four days on large surface area (225 mm^2) conductive ITO:PET substrates using potassium ferricyanide as a redox probe [33,34]. Monitoring biofilm over large scale (mm^2-cm^2) overcomes the local heterogeneity and the statistical issues encountered at smaller areas (μm^2) [35]. Additionally, larger areas allow for the flexible substrate to be bent, curved, or deformed to assume a number of different geometries. We thus investigated the influence of shape and curvature of ITO:PET sheets on the impedance with and without biofilms. The influence of bacterial viability and EPS exopolysaccharides on the biofilm impedance was also investigated by inactivating with sodium azide and carbonyl cyanide m-chlorophenyl hydrazone (CCCP) and using EPS component deleted mutants, Δpel and Δpsl respectively. This work presents a proof-of-concept for the rapid detection of a weak electroactive biofilm in the presence of an exogenous redox mediator, and lays out a framework of design considerations for future large surface ITO:PET flexible biofilm sensors.

2. Materials and Methods

Materials

ITO:PET (Thickness = 125 μm, surface resistivity = 60 Ω/sq., Sigma Aldrich, Singapore) sheets were used for all experiments. Coiled titanium wire and Ag/AgCl reference electrode (in saturated potassium chloride (KCl)) were obtained from Sigma Aldrich, Singapore and Latech scientific supply, Singapore, respectively. The chemicals used for bacterial growth included Luria-Bertani (LB, Becton Dickinson and Company, Singapore), ammonium sulphate ($(NH_4)_2SO_4$, Merck, Singapore), sodium phosphate, dibasic (Na_2HPO_4, Calbiochem, Singapore), potassium dihydrogen phosphate (KH_2PO_4, Merck, Singapore), sodium chloride (NaCl, Merck), magnesium chloride ($MgCl_2$, Merck, Singapore), calcium chloride ($CaCl_2$, Merck, Singapore), iron (III) chloride ($FeCl_3$, Sigma Aldrich, Singapore), glucose ($C_6H_{12}O_6$,

VWR chemicals, Singapore), sodium azide (NaN_3, Sigma Aldrich, Singapore) and CCCP (Sigma Aldrich, Singapore). Crystal violet (Sigma Aldrich, Singapore), absolute ethanol (Merck, Singapore), *Baclight* live/dead stain (Invitrogen, Thermo-Fisher, Singapore) and potassium ferricyanide (Sigma Aldrich, Singapore) were used for bacterial characterization.

ITO:PET geometry studies

The effect of geometry of ITO:PET was studied by varying the shape and aspect ratio of the sheets keeping the total surface area constant. The samples studied were 15x15 mm square sheet, 15x15 mm square sheet bent at the centre with ITO coating on the outer side, 20x11.25 mm rectangular sheet and 25x9 mm strip bent as a cylinder. Note that for the cylinder, an extra 10 mm was added and stapled for connecting each end of the strip. However, this staple was removed before any electrochemical measurements were conducted.

Bacterial strain and culture media

A non-mucoid wild type strain of *P. aeruginosa,* PAO1, (supplied by Dr. Celine Vidaillac, SCELSE, NTU) was used in all the experiments. For EPS study, PAO1 mutants, PAO1 Δpel and PAO1 Δpsl (supplied by Dr. Xinyi Zhu, SCELSE, NTU) were used. An overnight culture was grown in 10 mL of LB broth for 17 h at 37^{o}C and 200 rpm shaking. After growth, the overnight culture was centrifuged at 6000 rpm for 5 min and re-suspended in 10 mL ABTG medium which was prepared as previously reported without casamino acids and with 6.9 mM glucose as a main carbon source [36]. The same medium was used for biofilm growth experiments.

Biofilm growth experiment

ITO:PET sheets of all geometries/curvatures were cut, UV-sterilized and cleaned with 70% ethanol (v/v). For square and rectangle, the sheets were glued to the base of a petri dish with silicone sealant (Selleys, Singapore). In case of bent-square, the sheets were glued to petri

dishes using autoclave tape rolled as a cylinder whereas for cylinder, the stapled excess was glued to the petri dish. ABTG medium (15 mL for square and rectangle; 25 mL for bent square and cylinder) and PAO1 overnight culture were further added to obtain an initial optical density (at 600 nm wavelength) of 0.02. The difference in media volumes was to allow the sheets to be completely submerged in the media. Each petri dish consisted of two ITO:PET sheets. These dishes were incubated at 37^{o}C and 50 rpm shaking for 24-96 hours and the spent medium was replaced daily with fresh growth medium. At least three independent technical replicate biofilms were washed in fresh medium and tested at every time point (24, 48, 72, and 96 hours) to monitor the biofilm development.

Confocal Imaging of biofilms

Following biofilm growth for 24-96 hours, the square sheets were gently washed in fresh ABTG medium and stained with 4 µL *Baclight* live/dead stain. The samples were imaged by confocal laser scanning microscopy (Zeiss LSM 780 inverted microscope at 63x oil resolution) at four separate locations for each independent biological replicate. The obtained images were further quantified using COMSTAT 2 software (Technical University of Denmark, Kongens Lyngby, Denmark) [37] to obtain the live and dead biomass.

Crystal violet assay

After 24-96 hours, the square sheets were stained with 0.1% (v/v) crystal violet solution and washed with phosphate buffer saline (PBS) solution. 2 mL of absolute ethanol was added to the cleaned samples and the absorbance at 550 nm was measured with a microplate reader (TECAN M200, Switzerland).

Energy inhibitor treatment

Some of the biofilms grown for 72 hours on square sheets were further treated with sodium azide (NaN_3) and CCCP to inhibit energy production. For the NaN_3 study, the ABTG

medium was replaced by 50 mM NaN_3 dissolved in 20% (v/v) DI water in ABT (growth medium without glucose) and incubated at 37^{o}C and 50 rpm shaking for 4 hours. The control biofilm samples were treated with 20% (v/v) DI water in ABT. For CCCP experiments, the growth medium was replaced with 500 µM CCCP dissolved in 0.1% (v/v) DMSO and ABT. The samples were then incubated at 37^{o}C and 50 rpm shaking for 1 hour. For control experiments, the 72 hours grown biofilm samples were treated with 0.1% DMSO alone in ABT. Post-treatment, the samples were washed in ABTG to remove planktonic and loosely attached cells and electrochemical characterization was performed in ABTG as described above.

Electrochemical analysis

All experiments were conducted using a VSP or VMP3 multi-channel potentiostat (Bio-logic, France) in a three-electrode setup. ITO:PET sheets connected to a Pt sheet electrode holder (Latech, Singapore) were used as the working electrodes. Coiled titanium wire and Ag/AgCl were used as the auxiliary and reference electrodes respectively. During the electrochemical analysis, the headspace of the electrochemical cells was continuously flushed with high purity nitrogen gas to remove oxygen. The EIS analysis was carried out at open circuit potential (OCP) using the EC-Lab software (Bio-logic, France) in 10 mL fresh ABTG medium to keep the biofilm viable. The study was performed in the frequency range 100 kHz to 30 mHz with sinusoidal potential of 10 mV amplitude. For staircase potential EIS (SPEIS), a bias potential in the range to 50 mV to 500 mV was applied in addition to OCP in 50 mV steps. Potassium ferricyanide was added as an exogenous redox mediator. Three concentrations (1 mM, 5 mM and 10 mM) were studied and 5 mM was used as the optimum concentration for all the experiments (see Supplementary information).

The distribution function of relaxation time (DFRT) was analysed to determine the number of time constant exhibited by the biofilm-electrolyte system, thus justifying further modelling based on equivalent circuit methodology. The DFRT was extracted with impedance spectroscopy evolutionary programming software [38,39]. Following the DFRT analysis, the impedance data were fitted to an equivalent circuit model with the same number of time constant identified through DFRT to determine the interfacial resistance and constant phase element (CPE) for the biofilm/electrode interface using Z-Fit feature in the EC-lab software. Effective capacitance ($C_{eff)}$ at interface was calculated using the Hsu-Mansfeld equation [40] :

$$C_{eff} = \frac{(QR)^{1/\alpha}}{R}$$

Where,

Q = CPE (F $s^{(\alpha-1)}$), R = Charge transfer resistance (Ω), α = CPE coefficient

Statistical analysis

Statistical significance was analysed with one-way analysis of variance (ANOVA) followed by Tukey post-hoc test. A significance value of 0.05 was used to determine statistical significance. The statistics were calculated with respect to independent technical replicates (N).

3. Results and Discussion

Monitoring biofilm growth with CLSM and crystal violet method

CLSM and crystal violet assay were used to visualize and validate the biofilm growth and development on ITO:PET substrates at 24 hour intervals (Figure 1,2). After 24 hours growth (Figure 1a) there were few cells attached to the surface of the ITO:PET because the cells

were in the initial attachment stage. By 48 hours (Figure 1b), we observed a mix of individual cells and microcolonies; the cells began to irreversibly attach to the surface and initiated cluster formation. After 72 hours (Figure 1c) we obtained a mature biofilm, consistent with previous observations [41]. Continued growth beyond 96 hours resulted in a highly variable biofilm with a higher proportion of dead cells. (Figure 1d).

The biofilms formed were heterogeneous in structure as we observed variation of biomass at different locations on the same sample. This heterogeneity was presented as a mixture of flat and mushroom structures. Generally, mushroom structures form when glucose is the primary carbon source [42]. The mixture of flat and mushroom structures observed here are typically associated with biofilms grown on hydrophobic polymers [43]. Therefore, it was evident that the ITO:PET substrate contributed to the biofilm structure in our system.

The biofilm was further studied through quantitative analysis (Figure 2a) of the CSLM images to determine the biomass. The biomass of live cells (Figure 2a) increased from 0.03 ± 0.02 $\mu m^3/\mu m^2$ at 24 hours to 0.75 ± 0.07 $\mu m^3/\mu m^2$ at 72 hours and then decreased to 0.36 ± 0.12 $\mu m^3/\mu m^2$ after 96 hours. In contrast, the surface covered by the dead cells increased until 72 hours and stabilized at 96 hours. The biomass calculated from CSLM images correlated well with the crystal violet assay results (Figure 2b) , which similarly showed an increasing biomass up to 72 hours followed by decrease at 96 hours.

Effect of growth time on EIS analysis

Here, we used EIS to measure the complex impedance of the biofilm across a broad range of frequencies in presence of 5 mM ferricyanide as we were unable to observe changes without an exogenous mediator (Figure S1). *P. aeruginosa* primarily undergoes EET via mediated electron transfer through secretion of redox-active mediators known as phenazines (e.g., pyocyanin) that are produced at various stages of biofilm development [44]. However,

phenazines in our system were either washed away along with the planktonic cells in the cleaning step or not sufficient to drive the EET as seen in figure S1. Therefore, ferricyanide ions were added as a redox mediator to enhance the electron transfer rate towards the electrode through ionic migration and conduction [45,46]. Alternatively, 2-hydroxy-1,4-naphthoquinone (HNQ), a quinone derivative was also studied [47]. However, addition of ferricyanide showed better EIS characteristics and was therefore used for subsequent experiments (Figure S2). 5 mM was considered the optimal concentration of ferricyanide after testing three concentrations on biofilms grown for 72 hours (Figure S3). These concentrations were deemed safe as we were unable to observe any toxicity from 5 mM ferricyanide on the biofilms (Figure S4). Thus, the subsequent experiments were conducted at this concentration.

Figure 3 shows representative Nyquist and Bode plots of EIS measurements of biofilms recorded every 24 hours to match the critical stages of the life cycle of the biofilm. The 0 hour curve in Figure 3 corresponds to blank ITO:PET electrode, i.e., an electrode without bacterial inoculum. Representative EIS data plotted as a Nyquist plot (Figure 3a) showed a depressed semicircle shape, which indicated non-ideal capacitance [20]. Both the real and imaginary component of the impedance decreased with growth time of the biofilm.

Representative Bode-phase plots (Figure 3b) shows the phase angle with respect to frequency. Here, the frequency regimes indicated the characteristic time of different electrochemical effects. EIS at low frequencies (30 mHz to 3Hz) represent charge transfer and double layer capacitance at the ITO:PET-electrolyte interface. In contrast, the features at medium (3 Hz to 1 kHz) and high (1 kHz to 100 kHz) frequencies represent the charge accumulation effects on the ITO:PET-electrode interface as seen in (Figure S5) and the resistive behaviour of the electrolyte solution to the applied AC signal, respectively [48]. Figure 3b showed gradual increase in the phase angle at the lower frequency regime. In

contrast, no appreciable changes in the impedance at either medium or high frequencies were observed, which was expected as the biofilm growth does not influence the ionic concentration in the system [20]. We noted that the phase angle never reached -90^{o} in all measurements, which suggested that large surface ITO:PET-electrolyte interfaces behaved as a CPE [20]. This was in agreement with the depressed semi-circular feature observed in the Nyquist plot.

To study the impedance components at each frequency, the DFRT of the ITO:PET-biofilm system was calculated. Generally, DFRT curves comprise of distinct peaks that correspond to the different electrochemical phenomena in the system [49]. The location and shape of the peaks indicate the characteristic time of said phenomena. Figure 3c shows representative DFRT plots for the various growth times. We observed two distinct peaks at approximately 1 s and 0.01 s. For the blank ITO:PET, the contribution of low frequency behaviour to the total impedance was approximately 20 times larger than the medium frequency behaviour. The area of the peaks at low relaxation time (0.01 s) did not change with the biofilm growth, while the area under the peaks at 1 s decreased with biofilm growth and maturation. The large difference between these two contributions indicated that the low frequency regime was dominant, and therefore we focused our future analysis on the behaviour at these frequencies.

The changes in impedance at the low frequency region of the EIS plots observed in the DFRT analysis were due to changes in: (i) charge transfer resistance (ii) diffusion related resistance and (iii) double-layer capacitance [50]. The charge transfer resistance corresponded to the charge exchange at the semiconductor-electrolyte interface to equilibrate the redox potential of the ferricyanide and the Fermi energy of ITO, whereas diffusion related resistance is a result of mass transport of ferricyanide to the electrode in order to reduce to ferrocyanide [20,51]. ITO, an n-type degenerate semiconductor, formed a space charge layer in response to EIS [52]. The accumulation of the majority charge carriers in the space charge region gave

rise to the capacitance at the low frequency [53]. As CPE was used for the modelling, capacitance was calculated using Hsu-Mansfeld equation. This equation was applicable for our case because (i) CPE and resistance in were parallel in equivalent circuit, (ii) normal distribution of time constant were observed in DFRT and (iii) CPE coefficient, α ranged between 0.65 and 1 [13,54]. It is to be noted that the margin of error for capacitance calculation were higher for values with $\alpha < 0.7$.

Since the DFRT analysis showed two distinct time constants, a Randles equivalent circuit with two resistor-CPE circuits (Figure 3d) was chosen to represent the electrochemical system, with one additional resistor in series to account for the resistance in the solution [55]. The data modelled using both series and nested parallel equivalent circuit showed similar trend in the electrochemical behaviour (Figure S6). Despite this similarity, the subsequent results were fit using the series circuit shown in figure 3d, which we believed that the electrode-biofilm interface, electrode/biofilm-solution interface, and solution behaviour in series as depicted in the normal distributions in DFRT plot was the best physical representation of the system. Here, charge transfer and diffusion related effects, (from here on known as interfacial resistance) at electrode-biofilm interface were combined to simplify the circuit and apply Hsu-Mansfeld equation [20,40]. Moreover, as no change was observed at the high and medium frequency in figure 3b, the following results describe the features of the time constant at low frequency.

Figure 4 shows the interfacial resistance and effective capacitance from the fitted EIS results with respect to the biofilm growth time. The interfacial resistance decreased substantially compared to blank ITO:PET in the first 24 hours. This marked drop in interfacial resistance indicated the potential to detect the initial attachment and formation of biofilms. Although no significant difference was observed between 24 and 96 hours (Figure 4a), a decreasing trend was evident. Additionally, there was an evident transition from a more variable decrease in

interfacial resistance at 24 hours to a robust decrease at 96 hours (as seen from the scatter plot), which suggested that the electrochemical signature of the biofilm was more repeatable for more developed biofilms on the ITO:PET substrate. From these observations, we hypothesized that the change in interfacial resistance was correlated to the interactions of ferricyanide with bacteria attached to the electrode. In stark contrast to the interfacial resistance, effective capacitance, extracted from CPE changed minimally with time (Figure 4b). No substantial change in capacitance was observed as the effect of the ITO was dominant and masked the contribution from the biofilm. As a result, ITO:PET was insensitive to the thickness of the biofilm after initial attachment.

In this work, we conducted a frequency sweep across a broad range in contrast to continuous monitoring of *P. aeruginosa* biofilms at a single frequency since the dominant frequency range of EIS behaviour on ITO:PET films has not been studied before [11,22,56]. Our results identified 30 mHz to 3 Hz as the frequency range of interest and the interfacial resistance as the primary marker for the detection of bacterial growth.

Mechanism of biofilm sensing

Although we observed a difference in the resistive parameters at the electrode-biofilm interface after bacterial attachment, currently, there is limited knowledge of the *P. aeruginosa* component that participates in the electrochemical interactions with ferricyanide. Both intracellular, (e.g., *Pseudomonas* cytochrome c- 551 oxidase) [57,58] and extracellular components (EPS) (e.g., polysaccharides, eDNA) [59] may have contributed to the EIS behaviour observed, though the key mechanisms remain unknown despite being crucial for understanding the EIS results. Therefore, we further investigated the role of intracellular and extracellular components.

To investigate the role of intracellular components, the biofilms were treated with energy production inhibiting chemical reagents that render the biofilms metabolically inactive. Two different types of energy inhibitors, sodium azide (NaN_3) and CCCP were studied to account for different energy production mechanisms. NaN_3 is a respiration inhibiting biocide that binds to the cytochrome oxidases in *P. aeruginosa* [22]. This binding ceases the energy production via oxidative phosphorylation. CCCP is a proton motive force inhibitor that blocks energy production in biofilms through disruption of the membrane potential [60].

EIS at OCP was measured for the NaN_3 and CCCP treated samples and compared to the behaviour of blank ITO:PET and their respective controls. The EIS results were fitted using the same two time constant equivalent circuit previously shown (Figure 3d). We focused on interfacial resistance effects as they were recognized as the biomarker for detection in our previous results. Figure 5 shows the charge transfer behaviour for NaN_3 (Figure 5a) and CCCP (Figure 5b) treated samples. We observed a change in the interfacial resistance between non-colonized and colonized ITO:PET sheets in both instances. The NaN_3 treatment showed minimal change compared to the control biofilm as seen in figure 5a. In contrast, CCCP treatment significantly increased the interfacial resistance (Figure 5b). These experiments indicated that there were several routes for interfacial electron transfer for *P. aeruginosa* biofilms. However, further investigation beyond the scope of this report will be needed to form a more complete understanding on the overall EET effects of biocides for *P. aeruginosa* biofilms.

Potentiostatic EIS at different potential was used in addition to EIS at OCP to measure faradaic current characteristics for viable biofilms and non-viable biofilms. The application of electrochemical potential drives the EET to occur at a higher rate, and increases the current as a result [32]. This helps differentiate the EET activity of viable and non-viable biofilms. The current output (Figure 5c) showed that NaN_3 treatment resulted in lower current output at any

potential compared to the control (untreated biofilm), yet, had a slightly higher current output than the blank electrode. For CCCP treatment (Figure 5d), the current output for the control biofilm and treated biofilm followed a similar trend as NaN_3 treatment. The difference between the treated sample and blank electrode, however, was insignificant. The variation in the x-axis was due to changes in OCP which was dependent on the electrode surface, biofilm growth, redox reaction kinetics, and the concentration of redox species at the interface [61,62]. Considering the changes after the energy inhibitor treatment in the biofilms, our results confirmed that treatment with inhibitory agents hindered the charge transfer capability of the biofilm.

Extracellular components such as the EPS are another potential contributor to interfacial resistance. To investigate the role of extracellular components, EIS analysis of *P.aeruginosa* mutants with deletion of either pel or psl exopolysaccharide was conducted. Figure 6a shows no change in the interfacial resistance of WT, Δpel, and Δpsl strains. Bacterial attachment and biofilm development has been shown to happen in the absence of either pel or psl, , which is consistent with the similar interfacial resistance observed in the WT and the two mutants [63] Here, phase of biofilm development may vary for the three strains considering the similar EIS signature between the initial attachment and the mature biofilm phase as seen in Figure 2a. For a better understanding, SPEIS at various potentials was conducted as shown in figure 6b. Here, only Δpsl showed a drop in current with respect to WT, while Δpel current output was very similar to WT. This observation was in agreement with previous studies where psl was determined to play a primary role in the biofilm development of non-mucoid PAO1 strains [64,65]. In summary, although significant changes were not observed at OCP, the SPEIS results at higher potential show that EPS components contributed to charge transfer. Despite this, all our studies were done at OCP to avoid the EIS characteristics

arising due to faradaic current at the electrode-liquid interface, particularly at low frequency [13].

Effect of geometry on biofilm sensing:

In addition to the growth of biofilm, the material and the surface area available for biofilm growth may affect the sensitivity and reliability of EIS monitoring. Considering that our ITO:PET substrate was flexible, we next conducted EIS analysis of ITO:PET for different shapes and geometries (Figure 7a) with and without biofilms present on the surface.

Figure 7b shows the interfacial resistance for different shapes of the ITO:PET electrode. EIS always measured a significant decrease in the interfacial resistance once a mature biofilm formed after 72 hours, irrespective of shape. The interfacial resistance across four days of biofilm growth for all of the geometries indicated similar trends (Figure S7). Interestingly, the rectangular shape appeared to be the most robust shape for the detection of the biofilm. In contrast, the cylindrical shape only measured a significant change in interfacial resistance after 72 hours. The difference in sensitivity and robustness between the rectangular and cylindrical shapes may be due to the differences in active surface area, i.e., the area that interacts with ferricyanide, despite having the same geometrical surface area.

Figure 7c shows the capacitance across the various geometries studied with and without biofilms present. From Figure 7c, we observed no significant difference in capacitance across all experimental conditions except rectangle. The change in the capacitance for the rectangular electrode was probably because the biofilm growth blocked the interaction of charges and electrode [19]. Similarly, the capacitance for each geometry except rectangle tested did not show any significant change across four days of biofilm growth (Figure S8).

Limitations

There are some limitations of our work. Although phenazines are the redox mediators in *P. aeruginosa*, their concentration in our system was not sufficient to drive the EET therefore, external redox probe was used for the study. The investigation of biofilm sensing mechanism is limited to the role of cytochrome oxidases and exopolysaccharides and the other components that may participate in the electrochemical interactions were not studied. For geometry studies, further investigation is required to determine the role of geometric surface area and active surface area. Despite these limitations, our results presented a step towards detecting biofilms in a more realistic scenario, where larger surface area polymeric substrates of various shapes with non-ideal electrochemical properties are common.

Conclusions

In conclusion, we have shown that EIS at open circuit potential is able to rapidly detect the static growth of *P. aeruginosa* biofilms across large surface areas of ITO-coated flexible polymeric films over extended periods of time up to 4 days. EIS of *P. aeruginosa* in the presence of potassium ferricyanide on flat squares of ITO:PET indicated a decrease in impedance of the biofilm with increasing growth time, which was mostly due to the decrease of interfacial resistance with biofilm development whereas the interfacial capacitance dominated by space charge effects of ITO showed minimal changes. Confocal image analysis and crystal violet assays showed a near-complete coverage of the substrate after 72 hours of growth. However, the sensitivity of EIS was limited to detecting bacteria on the ITO:PET surface and was not able to differentiate between the attachment and maturation phases. Further investigation of the mechanism for changes in interfacial resistance revealed that the effect was likely due to the combination of increased presence of extracellular components (e.g., EPS) and bacterial metabolic activity. Shape or curvature of the sensor showed no influence on the trend of interfacial resistance and effective capacitance of the ITO:PET after

biofilm growth, opening up the potential for bespoke sensors to accommodate non-uniform geometries found in biomedical and industrial applications.

Acknowledgements

The authors thank Assoc. Professor Scott Rice (Singapore Centre for Environmental Life Sciences Engineering, NTU) for his critical insights during the research. The authors also thank Mr. Yu Hao Foo and Mr. Noel Sng (School of Chemical and Biomedical engineering, NTU) and Ms. Janice Low (Singapore Polytechnic) for their help. This work was financially supported by Nanyang Technological University Start-Up Grant (M4081814) and Singapore Centre for Environmental Life Sciences Engineering (SCELSE), whose research is supported by the National Research Foundation Singapore, Ministry of Education, Nanyang Technological University and National University of Singapore, under its Research Centre of Excellence Programme. This research is also supported by the Singapore Ministry of Health's National Medical Research Council under its NMRC/OFYIRG/NOV006/2016.

Declaration of Interests:

The authors declare no competing interests.

References

[1] H.C. Flemming, J. Wingender, U. Szewzyk, P. Steinberg, S.A. Rice, S. Kjelleberg, Biofilms: An emergent form of bacterial life, Nat. Rev. Microbiol. 14 (2016) 563–575. doi:10.1038/nrmicro.2016.94.

[2] H. Flemming, J. Wingender, The biofilm matrix, Nat. Rev. Microbiol. 8 (2010) 623–33. doi:10.1038/nrmicro2415.

[3] P.S. Stewart, Mechanisms of antibiotic resistance in bacterial biofilms, Int. J. Med. Microbiol. 292 (2002) 107–113. doi:10.1078/1438-4221-00196.

[4] L. Wang, D. Fan, W. Chen, E.M. Terentjev, Bacterial growth, detachment and cell size control on polyethylene terephthalate surfaces., Sci. Rep. 5 (2015) 15159. doi:10.1038/srep15159.

[5] J.H. Merritt, D.E. Kadouri, G.A. O'Toole, Growing and analyzing static biofilms, in: R. Coico, T. Kowalik, J. Quarles, B. Stevenson, R. Taylor (Eds.), Curr. Protoc. Microbiol., J. Wiley & Sons, Hoboken, NJ, 2005: pp. 1B1.1-1B1.17. doi:10.1002/9780471729259.mc01b01s22.

[6] S. Chan, K. Pullerits, J. Riechelmann, K.M. Persson, P. Rådström, C.J. Paul, Monitoring biofilm function in new and matured full-scale slow sand filters using flow cytometric histogram image comparison (CHIC), Water Res. 138 (2018) 27–36. doi:10.1016/j.watres.2018.03.032.

[7] A. Rohde, J.A. Hammerl, B. Appel, R. Dieckmann, S. Al Dahouk, FISHing for bacteria in food - A promising tool for the reliable detection of pathogenic bacteria?, Food Microbiol. (2015). doi:10.1016/j.fm.2014.09.002.

[8] Z. He, F. Mansfeld, Exploring the use of electrochemical impedance spectroscopy

(EIS) in microbial fuel cell studies, Energy Environ. Sci. 2 (2009) 215–219. doi:10.1039/B814914C.

[9] R.P. Ramasamy, Z. Ren, M.M. Mench, J.M. Regan, Impact of initial biofilm growth on the anode impedance of microbial fuel cells, Biotechnol. Bioeng. 101 (2008) 101–108. doi:10.1002/bit.21878.

[10] J. Azeredo, N.F. Azevedo, R. Briandet, N. Cerca, T. Coenye, A.R. Costa, M. Desvaux, G. Di Bonaventura, M. Hébraud, Z. Jaglic, M. Kačániová, S. Knøchel, A. Lourenço, F. Mergulhão, R.L. Meyer, G. Nychas, M. Simões, O. Tresse, C. Sternberg, Critical review on biofilm methods, Crit. Rev. Microbiol. 43 (2017) 313–351. doi:10.1080/1040841X.2016.1208146.

[11] D. Gutirrez, C. Hidalgo-Cantabrana, A. Rodrïguez, P. Garcïa, P. Ruas-Madiedo, Monitoring in real time the formation and removal of biofilms from clinical related pathogens using an impedance-based technology, PLoS One. 11 (2016) 1–17. doi:10.1371/journal.pone.0163966.

[12] M.E. Hernandez, Extracellular electron transfer, Cell. Mol. Life Sci. 58 (2001) 1562–1571. doi:10.1007/PL00000796.

[13] X. Dominguez-Benetton, S. Sevda, K. Vanbroekhoven, D. Pant, The accurate use of impedance analysis for the study of microbial electrochemical systems, Chem. Soc. Rev. 41 (2012) 7228–7246. doi:10.1039/c2cs35026b.

[14] L. Shi, D.J. Richardson, Z. Wang, S.N. Kerisit, K.M. Rosso, J.M. Zachara, J.K. Fredrickson, The roles of outer membrane cytochromes of Shewanella and Geobacter in extracellular electron transfer, Environ. Microbiol. Rep. 1 (2009) 220–227. doi:10.1111/j.1758-2229.2009.00035.x.

[15] G. Reguera, K.D. McCarthy, T. Mehta, J.S. Nicoll, M.T. Tuominen, D.R. Lovley, Extracellular electron transfer via microbial nanowires, Nature. 435 (2005) 1098–1101. doi:10.1038/nature03661.

[16] E. Marsili, D.B. Baron, I.D. Shikhare, D. Coursolle, J.A. Gralnick, D.R. Bond, Shewanella secretes flavins that mediate extracellular electron transfer, Proc. Natl. Acad. Sci. 105 (2008) 3968–3973. doi:10.1073/pnas.0710525105.

[17] L.E. Doyle, E. Marsili, Weak electricigens: A new avenue for bioelectrochemical research, Bioresour. Technol. 258 (2018) 354–364. doi:10.1016/j.biortech.2018.02.073.

[18] L. Liu, Y. Xu, F. Cui, Y. Xia, L. Chen, X. Mou, J. Lv, Monitoring of bacteria biofilms forming process by in-situ impedimetric biosensor chip, Biosens. Bioelectron. 112 (2018) 86–92. doi:10.1016/j.bios.2018.04.019.

[19] T. Kim, J. Kang, J.H. Lee, J. Yoon, Influence of attached bacteria and biofilm on double-layer capacitance during biofilm monitoring by electrochemical impedance spectroscopy, Water Res. 45 (2011) 4615–4622. doi:10.1016/j.watres.2011.06.010.

[20] V.F. Lvovich, Impedance Spectroscopy: Applications to Electrochemical and Dielectric Phenomena, John Wiley & Sons Inc., Hoboken, New Jersey, 2012.

[21] T.Q. Nguyen, C. Breitkopf, Determination of diffusion coefficients using impedance spectroscopy data, J. Electrochem. Soc. 165 (2018) E826–E831. doi:10.1149/2.1151814jes.

[22] L. Pires, K. Sachsenheimer, T. Kleintschek, A. Waldbaur, T. Schwartz, B.E. Rapp, Online monitoring of biofilm growth and activity using a combined multi-channel impedimetric and amperometric sensor, Biosens. Bioelectron. 47 (2013) 157–163.

doi:10.1016/j.bios.2013.03.015.

[23] A.C. Ward, P. Connolly, N.P. Tucker, Pseudomonas aeruginosa can be detected in a polymicrobial competition model using impedance spectroscopy with a novel biosensor, PLoS One. 9 (2014) e91732. doi:10.1371/journal.pone.0091732.

[24] A. Shirakura, M. Nakaya, Y. Koga, H. Kodama, T. Hasebe, T. Suzuki, Diamond-like carbon films for PET bottles and medical applications, Thin Solid Films. 494 (2006) 84–91. doi:https://doi.org/10.1016/j.tsf.2005.08.366.

[25] C. Ioakeimidis, K.N. Fotopoulou, H.K. Karapanagioti, M. Geraga, C. Zeri, E. Papathanassiou, F. Galgani, G. Papatheodorou, The degradation potential of PET bottles in the marine environment: An ATR-FTIR based approach, Sci. Rep. 6 (2016). doi:10.1038/srep23501.

[26] A. Ahani, L. Saadati-Fard, A.M. Sodagar, F.A. Boroumad, Flexible PET/ITO electrode array for implantable biomedical applications, Proc. Annu. Int. Conf. IEEE Eng. Med. Biol. Soc. EMBS. (2011) 2878–2881. doi:10.1109/IEMBS.2011.6090794.

[27] K.A. Sierros, N.J. Morris, S.N. Kukureka, D.R. Cairns, Dry and wet sliding wear of ITO-coated PET components used in flexible optoelectronic applications, Wear. (2009). doi:10.1016/j.wear.2008.12.042.

[28] T. Nguyen, F.A. Roddick, L. Fan, Biofouling of water treatment membranes: A review of the underlying causes, monitoring techniques and control measures, Membranes (Basel). 2 (2012) 804–840. doi:10.3390/membranes2040804.

[29] P.S. Stewart, J.W. Costerton, Antibiotic resistance of bacteria in biofilms., Lancet. 358 (2001) 135–138. doi:10.1016/s0140-6736(01)05321-1.

[30] N. Høiby, T. Bjarnsholt, M. Givskov, S. Molin, O. Ciofu, Antibiotic resistance of

bacterial biofilms, Int. J. Antimicrob. Agents. 35 (2010) 322–332. doi:10.1016/j.ijantimicag.2009.12.011.

[31] S. Bayoudh, A. Othmane, L. Ponsonnet, H. Ben Ouada, Electrical detection and characterization of bacterial adhesion using electrochemical impedance spectroscopy-based flow chamber, Colloids Surfaces A Physicochem. Eng. Asp. 318 (2008) 291–300. doi:10.1016/j.colsurfa.2008.01.005.

[32] H. Ben-Yoav, A. Freeman, M. Sternheim, Y. Shacham-Diamand, An electrochemical impedance model for integrated bacterial biofilms, Electrochim. Acta. 56 (2011) 7780–7786. doi:10.1016/j.electacta.2010.12.025.

[33] L. Yang, Y. Li, AFM and impedance spectroscopy characterization of the immobilization of antibodies on indium-tin oxide electrode through self-assembled monolayer of epoxysilane and their capture of Escherichia coli O157:H7, Biosens. Bioelectron. 20 (2005) 1407–1416. doi:10.1016/j.bios.2004.06.024.

[34] S. Kim, H.W. Cho, K. Hong, J.H. Son, K. Kim, B. Koo, S. Kim, J.-L. Lee, Design of red, green, blue transparent electrodes for flexible optical devices, Opt. Mater. Express. 22 (2014) A1257–A1269. doi:10.1364/OME.4.001257.

[35] T.R. Neu, J.R. Lawrence, Innovative techniques, sensors, and approaches for imaging biofilms at different scales, Trends Microbiol. (2015). doi:10.1016/j.tim.2014.12.010.

[36] S.L. Chua, L.D. Hultqvist, M. Yuan, M. Rybtke, T.E. Nielsen, M. Givskov, T. Tolker-Nielsen, L. Yang, In vitro and in vivo generation and characterization of *Pseudomonas aeruginosa* biofilm–dispersed cells via c-di-GMP manipulation, Nat. Protoc. 10 (2015) 1165–1180. doi:10.1038/nprot.2015.067.

[37] M. Vorregaard, Comstat2 - a modern 3D image analysis environment for biofilms,

Math. Model. (2008).

[38] A.B. Tesler, D.R. Lewin, S. Baltianski, Y. Tsur, Analyzing results of impedance spectroscopy using novel evolutionary programming techniques, J. Electroceramics. 24 (2010) 245–260. doi:10.1007/s10832-009-9565-z.

[39] Y. Tsur, S. Baltianski, Analyzing impedance spectroscopy results, Rare Met. Mat Eng. 35 (2006) 452–454.

[40] C.H. Hsu, F. Mansfeld, Concerning the Conversion of the Constant Phase Element Parameter Yo into a Capacitance, Corrosion. 57 (2001) 747–748. doi:https://doi.org/10.5006/1.3280607.

[41] G. O'Toole, H.B. Kaplan, R. Kolter, Biofilm Formation as Microbial Development, Annu. Rev. Microbiol. 54 (2000) 49–79. doi:10.1146/annurev.micro.54.1.49.

[42] M. Klausen, A. Heydorn, P. Ragas, L. Lambertsen, A. Aaes-Jørgensen, S. Molin, T. Tolker-Nielsen, Biofilm formation by Pseudomonas aeruginosa wild type, flagella and type IV pili mutants, Mol. Microbiol. 48 (2003) 1511–1524. doi:10.1046/j.1365-2958.2003.03525.x.

[43] O. Rzhepishevska, S. Hakobyan, R. Ruhal, J. Gautrot, D. Barbero, M. Ramstedt, The surface charge of anti-bacterial coatings alters motility and biofilm architecture, Biomater. Sci. 1 (2013) 589–602. doi:10.1039/c3bm00197k.

[44] T. Seviour, L.E. Doyle, S.J.L. Lauw, J. Hinks, S.A. Rice, V.J. Nesatyy, R.D. Webster, S. Kjelleberg, E. Marsili, Voltammetric profiling of redox-active metabolites expressed by Pseudomonas aeruginosa for diagnostic purposes, Chem. Commun. 51 (2015) 3789–3792. doi:10.1039/C4CC08590F.

[45] K. Watanabe, M. Manefield, M. Lee, A. Kouzuma, Electron shuttles in biotechnology,

Curr. Opin. Biotechnol. 20 (2009) 633–641. doi:10.1016/j.copbio.2009.09.006.

[46] J. Kang, T. Kim, Y. Tak, J.H. Lee, J. Yoon, Cyclic voltammetry for monitoring bacterial attachment and biofilm formation, J. Ind. Eng. Chem. 18 (2012) 800–807. doi:10.1016/j.jiec.2011.10.002.

[47] C. Santoro, A.F. Mohidin, L. Lo Grasso, T. Seviour, K. Palanisamy, J. Hinks, F.M. Lauro, E. Marsili, Sub-toxic concentrations of volatile organic compounds inhibit extracellular respiration of Escherichia coli cells grown in anodic bioelectrochemical systems, Bioelectrochemistry. (2016). doi:10.1016/j.bioelechem.2016.02.003.

[48] M.E. Orazem, B. Tribollet, Electrochemical Impedance Spectroscopy, John Wiley & Sons Inc., Hoboken, New Jersey, 2008.

[49] A. Oz, D. Gelman, E. Goren, N. Shomrat, S. Baltianski, Y. Tsur, A novel approach for supercapacitors degradation characterization, J. Power Sources. 355 (2017) 74–82. doi:10.1016/j.jpowsour.2017.04.048.

[50] A.J. Bard, L.R. Faulkner, Electrochemical Methods: Fundamentals and Applications, second ed., John Wiley & Sons Inc., Hoboken, New Jersey, 2001.

[51] R. Memming, Semiconductor Electrochemistry, John Wiley & Sons Inc., Hoboken, New Jersey, 2001.

[52] H. Kim, C.M. Gilmore, A. Pique, J.S. Horwitz, H. Mattoussi, H. Murata, Z.H. Kafafi, D.B. Chrisey, Electrical, optical, and structural properties of indium-tin-oxide thin films for organic light-emitting devices, J. Appl. Phys. 86 (1999) 6451–6461. doi:10.1063/1.371708.

[53] A. Hassanzadeh, M.H. Habibi, A. Zeini-Isfahani, Study of electronic structure of tin-doped In2O3 (ITO) film deposited on glass, Acta Chim. Slov. 51 (2004) 507–527.

[54] B. Hirschorn, M.E. Orazem, B. Tribollet, V. Vivier, I. Frateur, M. Musiani, Determination of effective capacitance and film thickness from constant-phase-element parameters, Electrochim. Acta. (2010). doi:10.1016/j.electacta.2009.10.065.

[55] S.E. Astorga, L.X. Hu, E. Marsili, Y. Huang, Electrochemical signature of Escherichia coli on Ni micropillar array electrode for early biofilm characterization, ChemElectroChem. Accepted Article Manuscript (2019). doi:https://doi.org/10.1002/celc.201901063.

[56] J.B.J.H. Van Duuren, M. Müsken, B. Karge, J. Tomasch, C. Wittmann, S. Häussler, M. Brönstrup, Use of Single-Frequency Impedance Spectroscopy to Characterize the Growth Dynamics of Biofilm Formation in Pseudomonas aeruginosa, Sci. Rep. (2017). doi:10.1038/s41598-017-05273-5.

[57] D. Barber, S.R. Parr, C. Greenwood, The oxidation of Pseudomonas cytochrome c-551 oxidase by potassium ferricyanide, Biochem.J. 173 (1978) 681–690. doi:10.1042/bj1750239.

[58] N. Ohno, M.A. Cusanovich, Reaction of c-Type Cytochromes with the Iron Hexacyanides: Mechanistic Implications, Biophys. J. (1981). doi:10.1016/S0006-3495(81)84754-6.

[59] L.Y. Zheng, R.B. Congdon, O.A. Sadik, C.N.H. Marques, D.G. Davies, B.G. Sammakia, L.M. Lesperance, J.N. Turner, Electrochemical measurements of biofilm development using polypyrrole enhanced flexible sensors, Sensors Actuators, B Chem. (2013). doi:10.1016/j.snb.2013.03.097.

[60] T.T. Huynh, D. McDougald, J. Klebensberger, B. Al Qarni, N. Barraud, S.A. Rice, S. Kjelleberg, D. Schleheck, Glucose starvation-induced dispersal of pseudomonas aeruginosa biofilms is camp and energy dependent, PLoS One. 7 (2012).

doi:10.1371/journal.pone.0042874.

[61] X. Sheng, Y.P. Ting, S.O. Pehkonen, The influence of sulphate-reducing bacteria biofilm on the corrosion of stainless steel AISI 316, Corros. Sci. (2007). doi:10.1016/j.corsci.2006.10.040.

[62] J.H. Park, H. Zhou, S.J. Percival, B. Zhang, F.R.F. Fan, A.J. Bard, Open circuit (mixed) potential changes upon contact between different inert electrodes-size and kinetic effects, Anal. Chem. (2013). doi:10.1021/ac3025976.

[63] A. Ghafoor, I.D. Hay, B.H.A. Rehm, Role of exopolysaccharides in Pseudomonas aeruginosa biofilm formation and architecture, Appl. Environ. Microbiol. (2011). doi:10.1128/AEM.00637-11.

[64] K.M. Colvin, V.D. Gordon, K. Murakami, B.R. Borlee, D.J. Wozniak, G.C.L. Wong, M.R. Parsek, The pel polysaccharide can serve a structural and protective role in the biofilm matrix of Pseudomonas aeruginosa, PLoS Pathog. (2011). doi:10.1371/journal.ppat.1001264.

[65] L. Yang, Y. Hu, Y. Liu, J. Zhang, J. Ulstrup, S. Molin, Distinct roles of extracellular polymeric substances in Pseudomonas aeruginosa biofilm development, Environ. Microbiol. (2011). doi:10.1111/j.1462-2920.2011.02503.x.

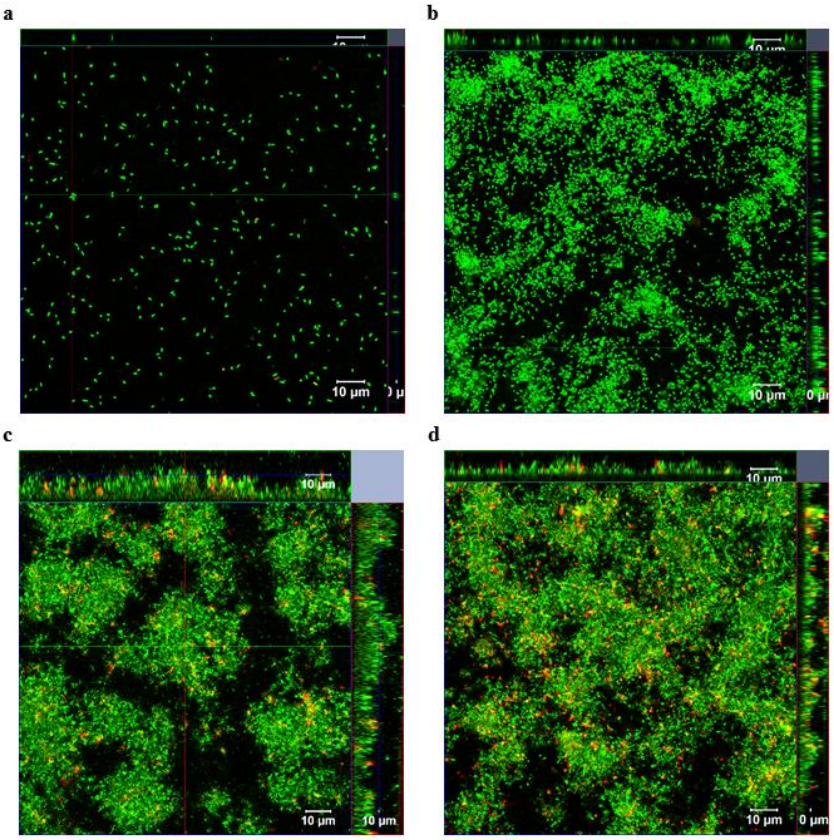

Figure 1: Representative CLSM orthogonal cross- sections at a: 24 hours b: 48 hours c: 72 hours and d. 96 hours growth.

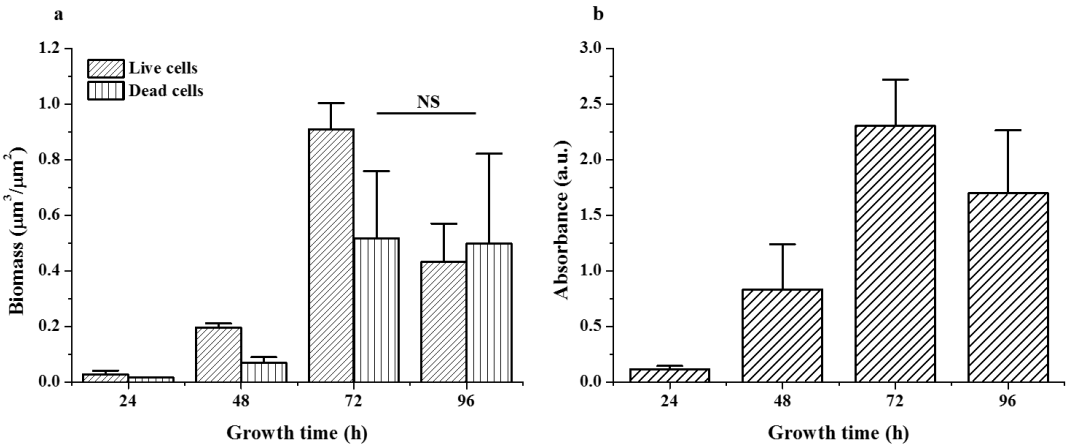

Figure 2: Live/dead biomass calculated by COMSTAT 2 (N=3, Mean ± SD). b: Crystal violet absorbance at 550 nm (N = 8, Mean ± SD), NS: statistically non-significant.

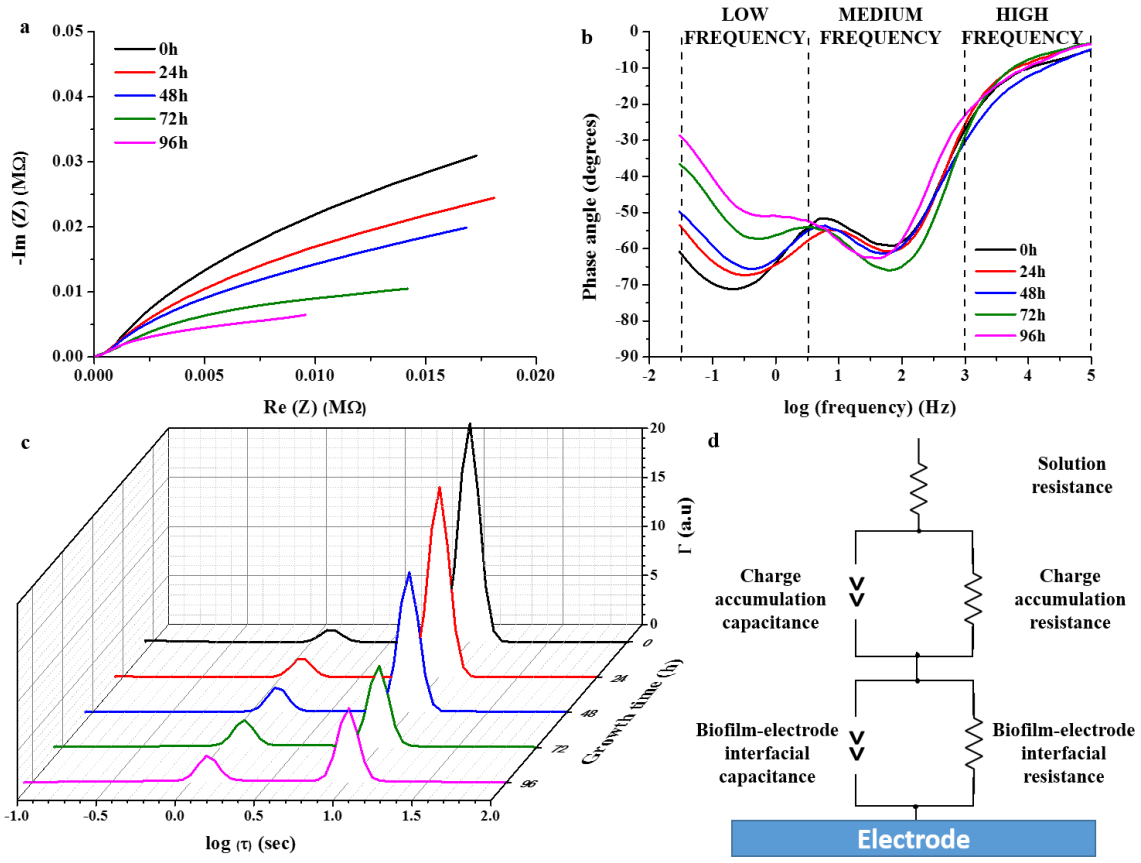

Figure 3: a: Representative Nyquist plot with respect to bacterial growth time b: Representative Bode phase plot with respect to bacterial growth time c: Representative DFRT plots for increasing growth time d: Schematic of equivalent circuit

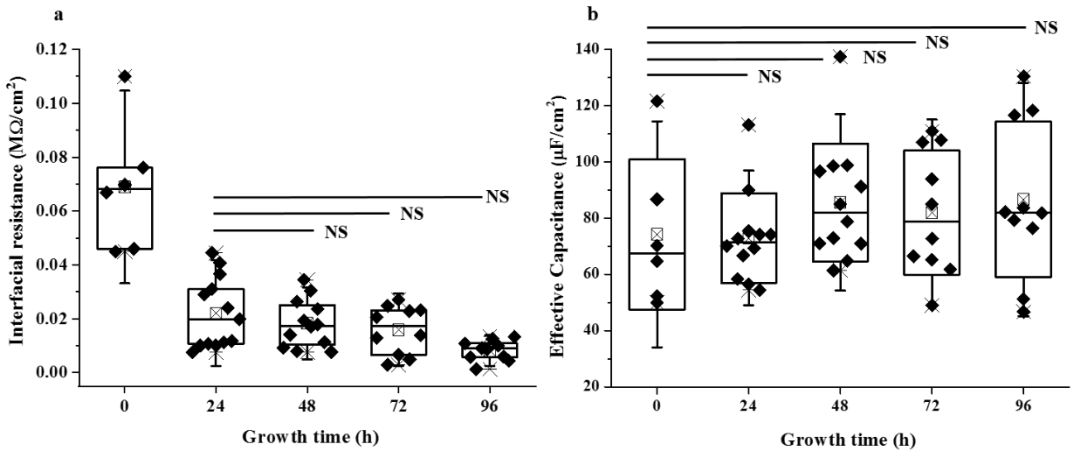

Figure 4: Interfacial resistance with respect to bacterial growth time and b: effective capacitance with respect to bacterial growth time.

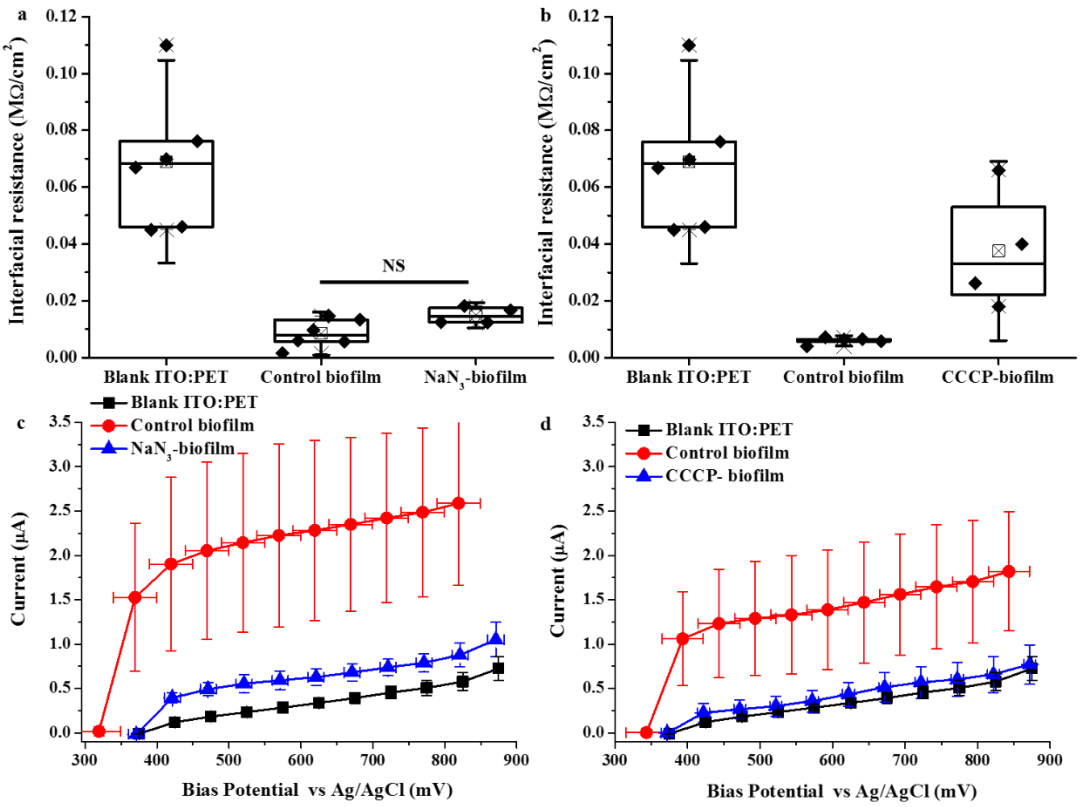

Figure 5: a: Interfacial resistance for blank ITO:PET, control biofilm and NaN_3 treated biofilm b: Interfacial resistance for blank ITO:PET, control biofilm and CCCP treated biofilm c: Current output at bias potential for blank ITO:PET (N=4, Mean ± SD), control biofilm (N=6, Mean ± SD) and NaN3 treated biofilm (N=4, Mean ± SD) d: Current output at bias potential for blank ITO:PET (N=4, Mean ± SD), control biofilm (N=5, Mean ± SD) and CCCP treated biofilm.

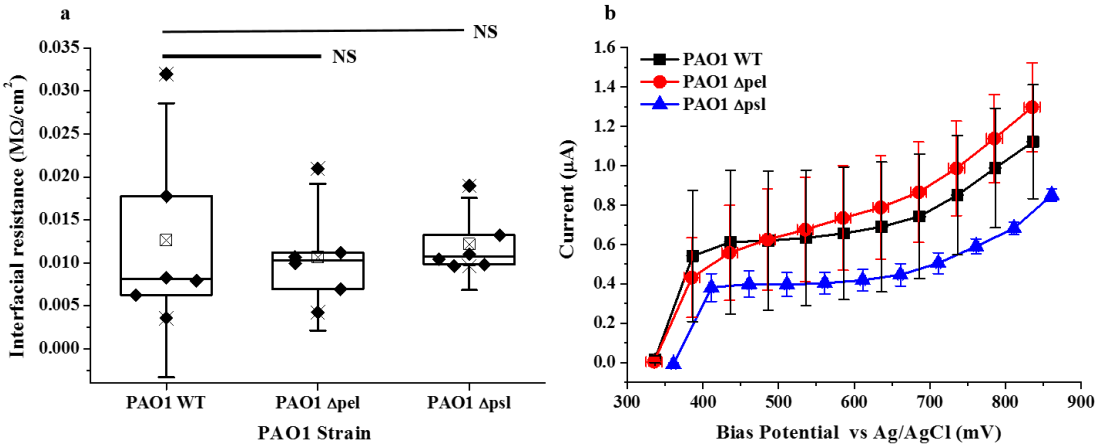

Figure 6: a: Interfacial resistance for WT and EPS mutant strains b: Current output at bias potential for WT and EPS mutant strains (N=6, Mean ± SD)

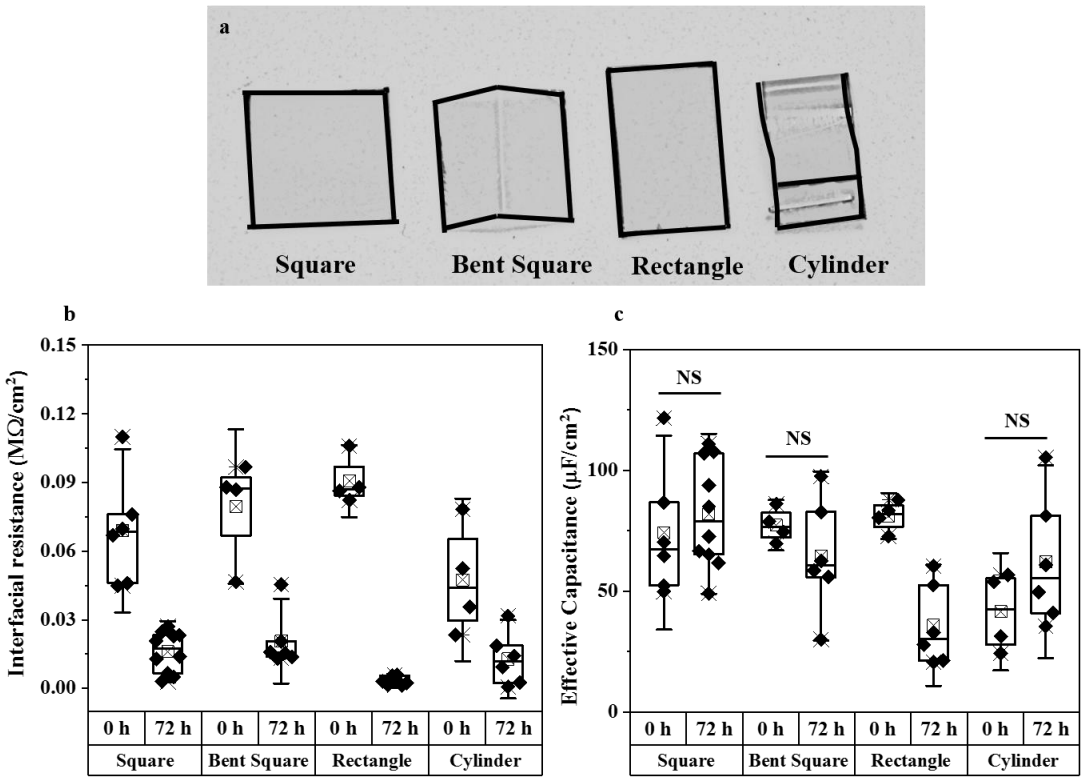

Figure 7: a: Schematic representation of electrode shapes b: Interfacial resistance with respect to electrode shape and b: effective capacitance with respect to electrode shape.

Figure 1

Click here to download high resolution image

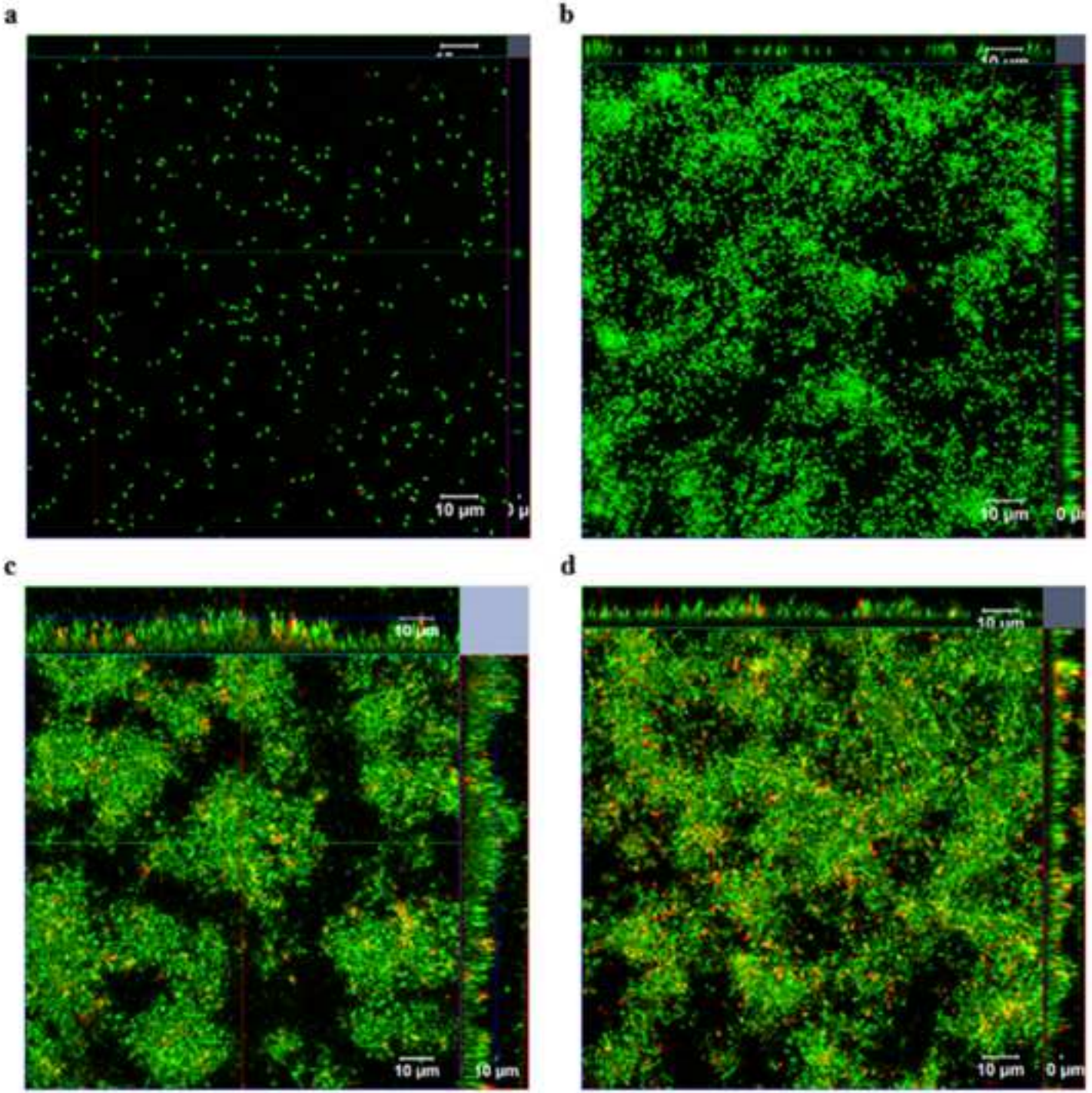

Figure 2

Click here to download high resolution image

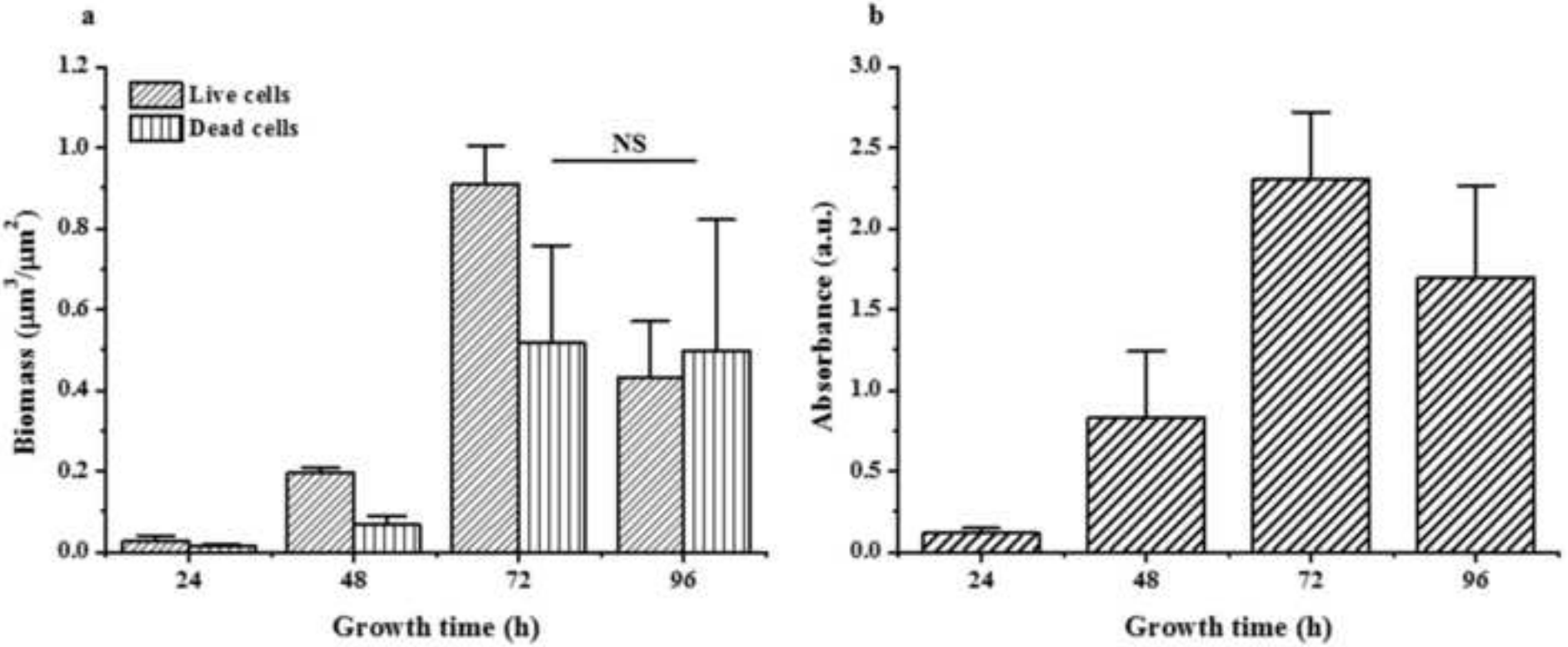

Figure 3

Click here to download high resolution image

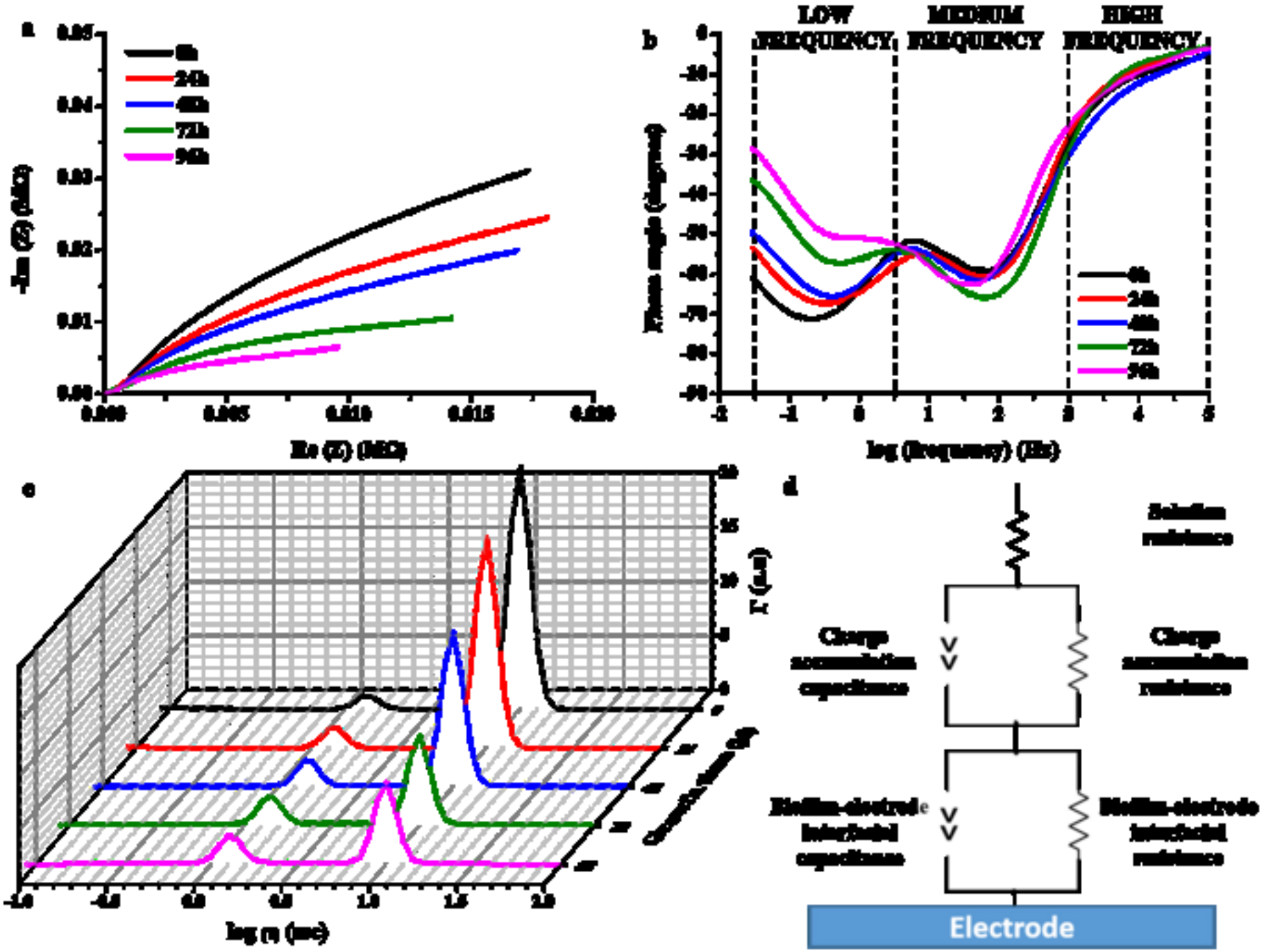

Figure 4

Click here to download high resolution image

Figure 5

Click here to download high resolution image

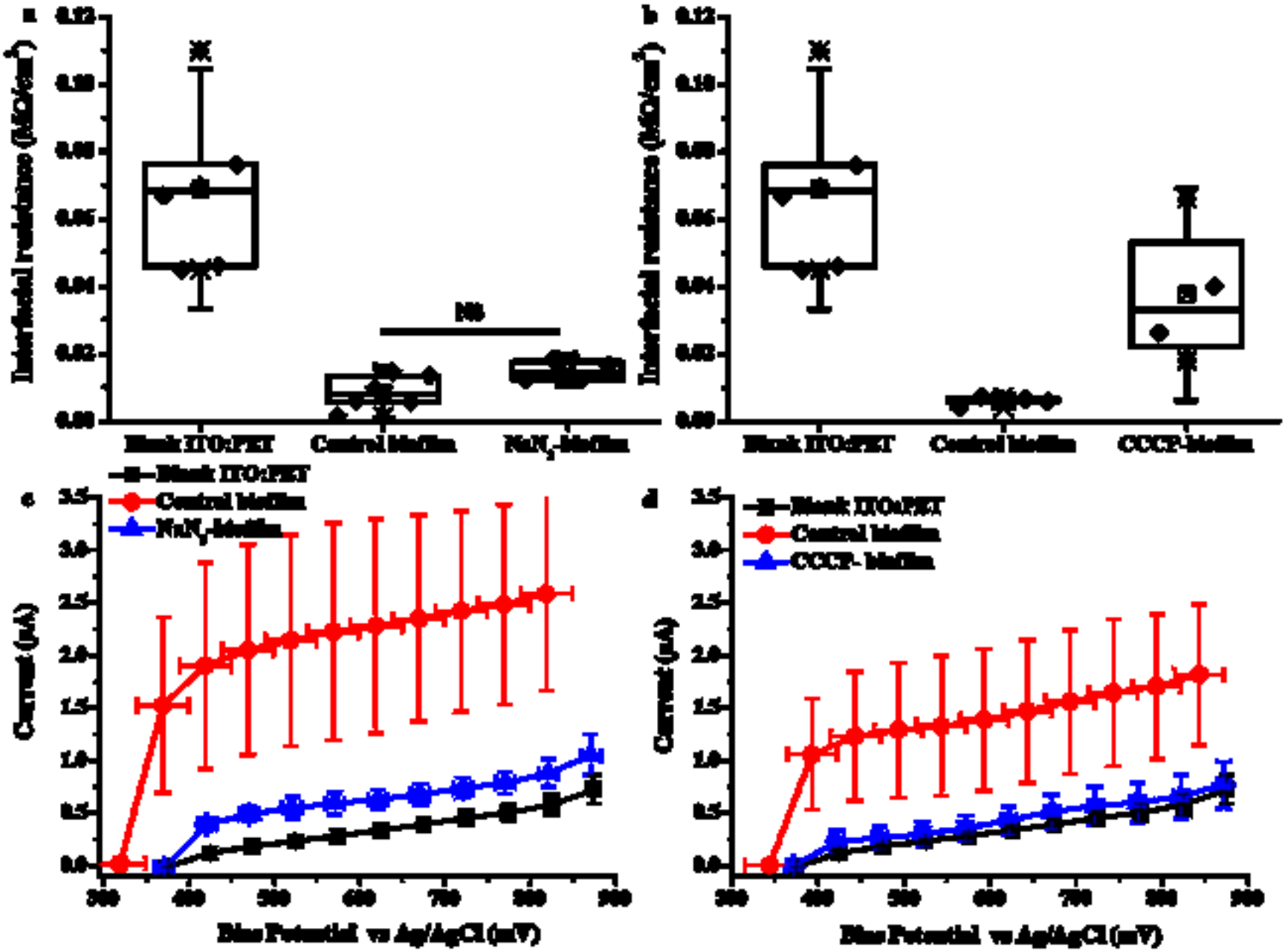

Figure 6

Click here to download high resolution image

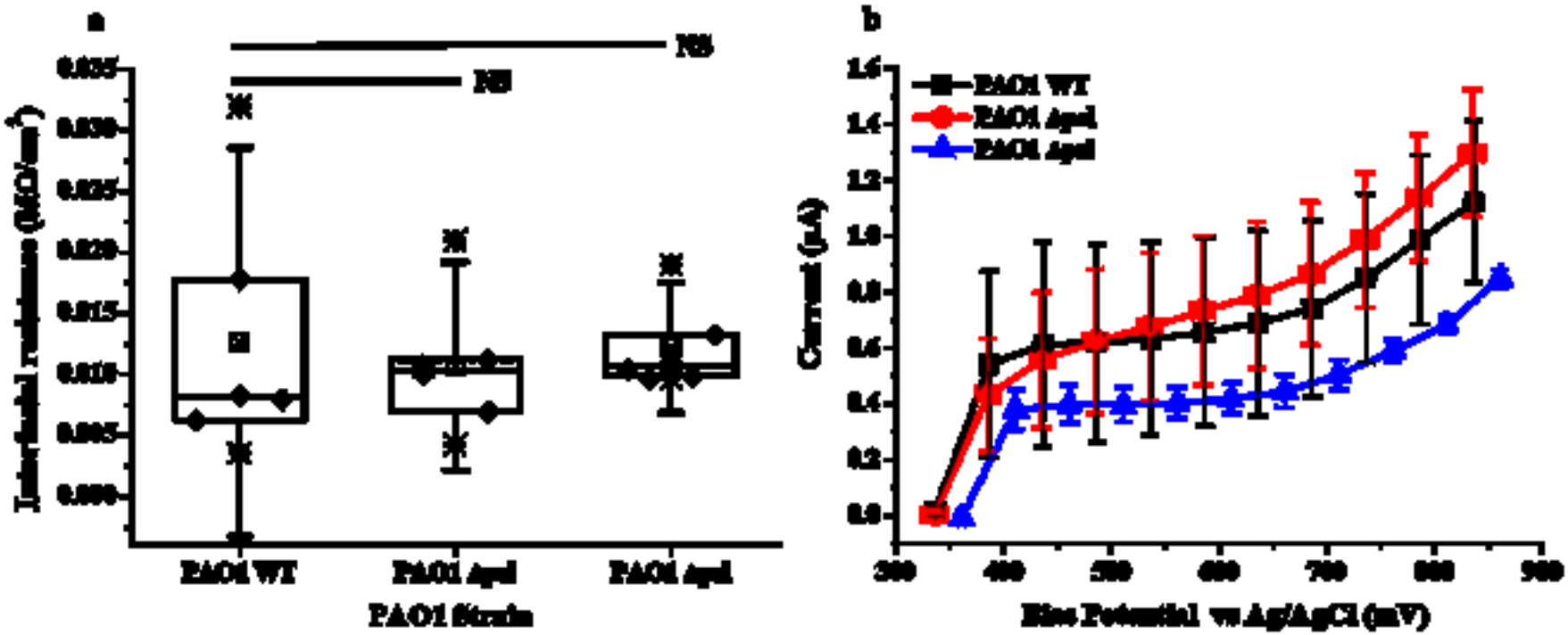

Figure 7

Click here to download high resolution image

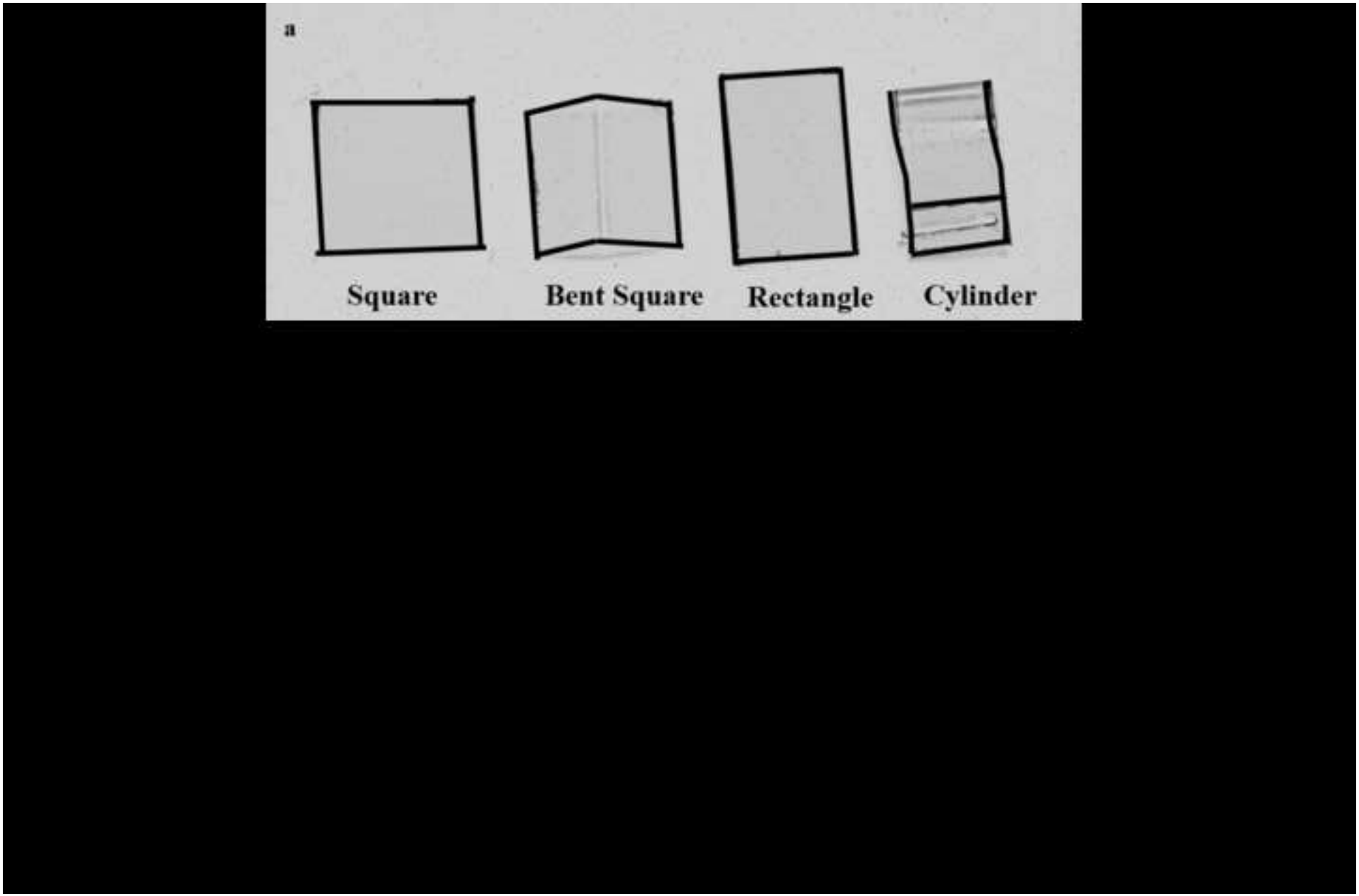

Supplementary Materials

Click here to download Supplementary Materials: ElectrochemicalDetection_Supplementary Information_LDB.docx

HIGHLIGHTS:

- *P. aeruginosa* biofilms were grown on polymeric substrate over large surface area
- Electrochemical impedance spectroscopy was tested to monitor biofilm development
- Charge transfer resistance detects the inception of biofilm maturation
- Impedance results correlate with confocal microscopy and crystal violet assay
- Both cells and matrix components contribute to EET